Implicit Algorithm for Brownian Dynamics of Polymers†

Marshall Fixman

Department of Chemistry, Colorado State University, Fort Collins, Colorado 80523.
Received October 7, 1985

ABSTRACT: Am implicit algorithm for the simulation of Brownian dynamics with hydrodynamic interaction is presented. The large time steps and rapid execution time of constrained polymer simulations are retained in combination with an approximately valid treatment of vibrational motion. The main advantage over previous approaches lies in the flexibility of the method. Because the chain is held together with a vibrational potential rather than by constraints, a trajectory may be followed with large time steps and approximately correct vibrational motion, or small time steps and accurate vibrational motion. Illustrative tests of the method are presented for chains with strong nonbonded interactions, with and without hydrodynamic interaction. The computation for one large time step using the implicit algorithm is about 2–4 times greater than for explicit algorithms that use short time steps, the penalty decreasing with increasing chain length. However, the time step may be 25–50 times longer than with the explicit methods, so that the computation time for a trajectory of given duration is reduced by a factor exceeding 6.

1. Introduction

The vibrational motion of polymer chains takes place on a much shorter time scale than that of the conformational motion, which is usually the subject of interest in a computer simulation. To avoid the very short time steps required by the vibrational motion, constraints on bond lengths and angles have been introduced into the simulation of Langevin's[1-3] or Newton's[4-6] equations of motion. Alternatively, the vibrational force constants can be weakened in order to permit a somewhat longer time step.[7] A third possibility, the use of implicit methods to solve the equations of motion for large time steps, is considered here for the case of Langevin or Brownian dynamics. The method is analogous to the algorithms used for "stiff" deterministic differential equations.[8-10]

We begin with a brief summary of the behavior of the implicit algorithm. If the product of vibrational force constants f and time step τ (taken in the appropriate reduced units) is large, then a solution of the implicit equations for coordinate displacements gives results nearly equivalent[11] to those obtained when constraints are imposed on bond lengths and angles.[1] A compensating metric potential[1,3,12,13] is then required to cancel the shift in dihedral angle distribution induced by the constraints. If the product $f\tau$ is small, an iterative solution gives results equivalent in first order to a simple Euler solution[14] and in second order to a Runge–Kutta algorithm.[15] For large time steps the vibrational force constants generate vibrational fluctuations in approximate agreement with proper values, and may be adjusted for improved agreement. This flexibility affords an advantage over constraints in some applications. The computation time for a single step along a trajectory is roughly a factor of 4 larger for the implicit algorithm than for the explicit Runge–Kutta algorithm, for short chains or chains without interactions between nonbonded atoms. The penalty factor drops to ~ 2 for 50-atom chains with nonbonded interactions. The time step may be larger by a factor of 25–50, depending on how much the vibrational potentials have been softened from realistic values, so the net gain in computational efficiency ranges from about 6 to 25.

The present work is concerned solely with motion of the backbone atoms. If substituent groups are present and are rigidly affixed to the backbone, the potential energy of the chain remains a function of the backbone coordinates and no significant modification of the approach is required. However, if the substituent groups are flexible, i.e., if time-dependent coordinates in addition to the backbone coordinates are required to specify their positions, then considerable reworking of the algorithm might[16] be required to maintain efficiency in the calculation. The efficiency of solving the coupled equations for coordinate displacements is highly dependent on the fact that the strong vibrational forces in the backbone give rise to a coupling matrix with a narrow band structure. Methods[4-6] based on constraints that do not take advantage of this feature, which is also found in the cooresponding constraint force matrix,[1] are relatively inefficient.

The general point of view and main problems are discussed in an elementary way and illustrated with simple examples in section 2, and the details are developed in section 3. Tests of the approach are reviewed in section 4. A few topics are considered in section 3, namely the use of "lumped" hydrodynamic interaction and the inclusion of internal friction, that have more to do with the theme of increased computational speed than with implicit algorithms. However, these devices were not employed in the algorithm that was actually tested.

In the concluding discussion, section 5, a recent application of the implicit algorithm to interacting chains is discussed.

2. General Approach

In this section a simple form of the equations of motion is used to illustrate the approach. Complicating factors, such as hydrodynamic interaction, are deferred to section 3. Most of the discussion concerns the Langevin equation, but the possibility of a similar treatment of Newton's equation is considered very briefly.

The analysis concerns particularly the change in configuration of a dynamical system during a time step τ, taken along an arbitrary trajectory. The magnitude of τ is said to be large or small in comparison with the smallest relaxation time of vibrational fluctuations; both extremes are considered.

The discussion of large time steps proceeds, usually implicitly, as if τ were also much larger than the largest relaxation time of the vibrations. In other words, the implicit assumption is that a large gap exists in the spectrum of relaxation rates between vibrations on the one hand and all conformational motions on the other. For the purpose of mathematical theory, such a gap can be achieved for any system of arbitrary but fixed size, through a limiting process in which vibrational force constants are taken arbitrarily large. However, this sort of justification does not give much assurance that the methods are actually applicable for large τ to systems with finite vibrational

† Supported in part by NIH GM27945.

0024-9297/86/2219-1195$01.50/0

amplitudes. That question is considered to be a practical one and is intended to be answered, at least partially, by the results presented in section 4.

A. Brownian Simulation. The Langevin equation has the schematic form

$$dx/dt = G(x) + \mathcal{L}(t) \tag{2.1}$$

where $x(t)$ is the position of the system in coordinate phase space, $G(x)$ is a potential force, and $\mathcal{L}$ is the random force. Appropriate units are assumed to have been used to eliminate a friction constant and k_BT. In a time step τ the system passes from an initial position $x^0 = x(0)$ to a final position $x = x(\tau)$, and

$$x - x^0 = \tau\bar{G} + (2\tau)^{1/2}L \tag{2.2}$$

L is a random displacement of zero mean and unit variance, and $\bar{G}$ is the time average of $G(x)$ over the interval τ.

Three approximate integration rules[9] have been considered for $\bar{G}$: the "trapezoidal" rule (TR), the "midpoint rule" (MP), and the "backward Euler" rule (BE)

$$\bar{G} \equiv \tau^{-1}\int_0^\tau G(x)\, dt \tag{2.3}$$

TR Rule

$$\bar{G} \cong \tfrac{1}{2}[G(x^0) + G(x)] \tag{2.4}$$

MP Rule

$$\bar{G} \cong G(\bar{x}) \tag{2.5}$$

$$\bar{x} \equiv \tfrac{1}{2}(x^0 + x)$$

BE Rule

$$\bar{G} \cong G(x) \tag{2.6}$$

The different components of $G(x)$, such as the vibrational force and the nonbonded atom force, may be treated by different rules; for large τ the components were so treated.

I. Large τ. The TR and MP rules are frequently used for systems of "stiff" differential equations.[8,9] They are not much different in practice, although the MP rule works somewhat better for strong repulsive interactions between nonbonded atoms. We used one or the other in all applications but one. For large τ, the time-average vibrational force is evaluated according to the BE rule, eq 2.6, because it proves more stable than the other rules and because its physical consequences seem less objectionable.

The physical consequences to which we allude are easily illustrated for a single particle moving in a one-dimensional vibrational well

$$G(x) \equiv -fx \tag{2.7}$$

The solutions of eq 2.2 for the TR and BE rules are

TR

$$x = (1 + \tau f/2)^{-1}[(1 - \tau f/2)x^0 + (2\tau)^{1/2}L] \tag{2.8}$$

BE

$$x = (1 + \tau f)^{-1}[x^0 + (2\tau)^{1/2}L] \tag{2.9}$$

For the harmonic force being considered, the TR and MP rules are the same. For a time increment much larger than the vibrational relaxation time f^{-1}, the TR rule makes x a Gaussian variable with mean $-x^0$ and variance $8/(\tau f^2)$. The BE rule makes the mean vanish and sets the variance to $2/(\tau f^2)$. Ideally, the system (2.7) should exhibit vibrational equilibration after a time much larger than f^{-1}. That is, x should follow the Boltzmann distribution and have vanishing mean and variance f^{-1} in units such that $k_BT = 1$. We suppose that the observed instability of the TR rule for large τf is due to a tendency to make x oscillate between x^0 and $-x^0$ after successive large time steps.

Neither integration rule gives the correct dependence of the long-time variance of f, and both rules improperly make the variance dependent on τ. For large τf, the variance is much less than its proper value, f^{-1}. This error might seem inconsequential in studies of conformational relaxation; however, dynamical simulations induce a correlation between vibrational and conformational degrees of freedom that has to be recognized. A detailed analysis given previously[1] for constrained Langevin dynamics showed that the correlation could be fully compensated by addition of a special metric potential to the potential energy of the system. This potential is $2^{-1}\ln h$, where h is the determinant of a band matrix discussed previously.[1,12] Since the present algorithm in the limit of large f yields displacements that are identical with those calculated with constraints, a necessity for compensation has to be expected. Several tests of the compensation will be discussed in section 4. Others have been reported[3,17] in connection with the direct imposition of constraints.

In practice, one not only can compensate the undesired correlation between vibrational and conformational degrees of freedom and the consequent shift in conformational weights but also can come close to realistic values for the vibrational amplitudes by choosing vibrational force constants somewhat smaller than their proper values. That is, the force constants f_D used for the dynamical simulations can be set to smaller values than the f_E used for Monte Carlo (equilibration) simulations, and the corresponding vibrational amplitudes can be matched. This also will be illustrated in section 4. We find that $\tau f_D > 2$ is a sufficient condition for the compensation of conformational shifts by the metric potential to have adequate numerical accuracy.

An explicit solution of eq 2.2 for x is not generally possible. However, an iterative method of the Newton–Raphson type[9] has been found to work quite well. It will be outlined in section 3.

II. Small τ. To first order in τ, the displacement is obtained from eq 2.2 with the approximation $\bar{G} = G(x^0)$

$$x_1 = x^0 + \tau G(x^0) + (2\tau)^{1/2}L \tag{2.10}$$

This is what we have called the Euler algorithm, in accordance with usage for deterministic equations.[9]

A second-order solution can be obtained by iteration of the Euler approximation in the TR rule, eq 2.4

$$\bar{G}_1 \equiv \tfrac{1}{2}[G(x^0) + G(x_1)] \tag{2.11}$$

$$x_2 = x^0 + \tau\bar{G}_1 + (2\tau)^{1/2}L \tag{2.12}$$

Equation 2.12 is equivalent to the Runge–Kutta second-order rule used by Helfand, et al.[7,15] (The second-order Runge–Kutta method is sometimes called Heun's method, in distinction to the more common fourth-order rule used for deterministic equations[9]. The deterministic rule follows from $L \to 0$.) Equation 2.12 is no longer implicit; the iterations are accomplished explicitly, in contrast to what is necessary for large τ.

B. Newtonian Simulation. Newtonian simulations have not been carried through to the program stage. This brief discussion is included only to indicate the possibility of a development similar to that introduced above. Let

$$m\bar{a} = \bar{G} \tag{2.13}$$

where m is the mass, $\bar{a}$ is the time average of the acceleration over an interval $(-\tau, \tau)$, and G is again the time average of the potential force, now taken over $(-\tau, \tau)$. It seems natural to take

$$\bar{a} \equiv (2\tau)^{-1}[\dot{x}(\tau) - \dot{x}(-\tau)] \quad (2.14)$$

$$\simeq (2\tau^2)^{-1}[x(\tau) + x(-\tau) - 2x(0)] \quad (2.15)$$

because the popular and effective Verlet algorithm[18] is then recovered for small τ. Furthermore, Ciccotti et al.[6] have successfully used the central difference formula (2.15) with constraining forces. It therefore seems probably that it would be adequate here, with G again estimated by a combination of the TR or MP rule for nonbonded forces and the BE rule for vibrational forces. It also seems probable that these rules would show some of the same effects found above for Langevin simulation. That is, the TR or MP rule applied to vibrations with large τf would give unstable oscillation. The BE rule should be relatively stable but would make the vibrational amplitudes much smaller than their equilibrium expections. Consequently a compensating metric potential would again be required.

3. Algorithm for Brownian Dynamics

A. Differential Equations. We begin with a summary of standard equations.[1,14,19] In addition, two modifications are briefly considered that would be useful in some applications: the lumping of centers of friction for the purpose of treating hydrodynamic interaction, and the incorporation of internal friction in lieu of realistic backbone potential energies. These modifications are relevant to the theme of increased computational efficiency rather than to the use of implicit algorithms per se, and neither modification was used for the simulations described in section 4.

The total force $\mathbf{F}_i^{\mathrm{T}}$ on bead i, $i = 0, ..., M$, is compounded of a hydrodynamic or external friction force $-\mathbf{F}_i^{\mathrm{H}}$, an internal friction force $\mathbf{F}_i^{\mathrm{I}}$, a potential force $\mathbf{P}_i$, and a random force $\mathcal{R}_i$

$$F^{\mathrm{T}} = -F^{\mathrm{H}} + F^{\mathrm{I}} + P + \mathcal{R} \quad (3.1)$$

The symbols without subscripts stand for column arrays. The total force is assumed to vanish; i.e., inertia is supposed negligible. The individual terms in eq 3.1 are defined in more detail as follows.

I. Hydrodynamic Force F^{H}. The hydrodynamic force F^{H} imposed by the beads on the solvent is

$$F^{\mathrm{H}} = \beta(V - V') \quad (3.2)$$

where

$$V' = V^0 + TF^{\mathrm{H}} \quad (3.3)$$

β is a diagonal array of friction constants, V is the array of bead drift velocities, and V' is the perturbed solvent velocity. V' is composed of the unperturbed velocity V^0 and perturbations $\mathrm{T}_{ij}\cdot\mathbf{F}_j^{\mathrm{H}}$. The latter result from a force $\mathbf{F}_j^{\mathrm{H}}$ imposed at the position $\mathbf{R}_j$ of bead j. Equations 3.2 and 3.3 give

$$F^{\mathrm{H}} = H^{-1}(V - V^0) \quad (3.4)$$

where

$$H \equiv \beta^{-1} + T \quad (3.5)$$

Ordinarily H^{-1} would be designated a frictional resistance matrix and H a diffusion matrix. Retention of internal friction would modify the significance of this terminology.

A few words about the practical treatment of T_{ij} seem appropriate here. For large $\mathbf{R}_{ij}$, T_{ij} approaches the Oseen interaction. We have used the Rotne–Prager approximation[20] in recent work.[21] Although slightly more complicated than the Oseen interaction, it offers several advantages: it gives a positive-definite and divergenceless H, it is reasonably accurate for spherical beads, and it has a meaningful extension to overlapping beads. It is unlikely that T_{ij} will ever be available to high precision for small $\mathbf{R}_{ij}$. The continuous solvent model then becomes suspect. Even if it is accepted, the hydrodynamic interactions are not strictly additive. And even if nonadditive interactions are ignored, the hydrodynamic interaction (HI) is difficult to obtain precisely for beads of complex shape. Given the further observation that either the square root or a triangular factorization of the HI matrix H is required in the computation of the Langevin forces, it would usually be desirable, and might be adequate, to lump the beads into consecutive groups for the purpose of computing T_{ij} or H_{ij} for $i \neq j$. This approximation reduces the size of the matrix operations involving H. We suggest

$$\mathrm{H}_{ij} = \mathrm{H}_{ij}^{\mathrm{B}} + \mathrm{H}_{IJ}^{\mathrm{G}} \quad (3.6)$$

where $I(i)$ and $J(j)$ label the groups to which i and j belong. $\mathrm{H}_{IJ}^{\mathrm{G}}$ is a dyadic function of the vector distance between group centers and has the same form as given in (3.5) but applies to groups of beads. H^{B} is a diagonal matrix and represents the extra diffusion of a bead within a group. It follows that H^{B}, H^{G}, and therefore also H, will be positive-definite.

II. Internal Friction Force F^{I}. The internal friction force F^{I} has been introduced in coarsegrained analytical approximations[22] as a substitute for a detailed treatment of rotational energy barriers to the motion of individual backbone atoms. It is assumed to have the form

$$F^{\mathrm{I}} = -QV \quad (3.7)$$

where Q is a square matrix of elements Q_{ij} that may be, like the T_{ij}, dyadic functions of position. If present, the Q_{ij} would be used to generate frictional forces along the vectors joining adjacent beads and would vanish except for $|i - j| = 1$. The energy of interaction between the two beads would be, in first approximation, the potential of average force. Thus

$$\mathbf{F}_i^{\mathrm{I}} = \alpha_{i+1}\mathbf{b}_{i+1}\mathbf{b}_{i+1}\cdot(\mathbf{V}_{i+1} - \mathbf{V}_i) + \alpha_i\mathbf{b}_i\mathbf{b}_i\cdot(\mathbf{V}_{i-1} - \mathbf{V}_i) \quad (3.8)$$

where

$$\mathbf{b}_i = \mathbf{R}_i - \mathbf{R}_{i-1} \quad (3.9)$$

and α_i may be a function of $|\mathbf{b}_i|$; $\alpha_0 = \alpha_{M+1} = 0$.

III. Potential Force P. The force P on any bead is a function of bead coordinates R. We have used pairwise additive potentials for all forces considered: vibrational, nonbonded, and metric potential forces (the latter forces are never strictly additive over pairs). As was remarked in the Introduction, any atoms at positions fixed by the backbone may also be centers of force, with the consequence that the backbone forces will no longer be pairwise additive.

In practice the forces were divided into two categories

$$P = P^{\mathrm{V}} + P^{\mathrm{E}} \quad (3.10)$$

where P^{V} is the vibrational force and P^{E} is everything else: excluded volume or nonbonded forces, external force, and metric potential force. This division was used to facilitate use of the TR or MP rule for the time average of P^{E} and the BE rule for P^{V}.

The vibrational forces were obtained from a potential energy

$$\tfrac{1}{2}f(R - R^{\mathrm{e}})^2 \quad (3.11)$$

where R is the distance between a pair of backbone beads, $(i, i + 1)$ for bond vibrations, or $(i, i + 1)$ for indirect control over bond angle vibrations. R^{e} is a corresponding equilibrium distance, and f is a corresponding force constant.

The constants f and R^e are of course different for adjacent and next nearest pairs of beads and in general vary with position along the backbone.

The metric potential part of P^E, say P^M, should in principle be calculated from[1,12]

$$P^M = -\nabla(\tfrac{1}{2} \ln h) \tag{3.12}$$

where h is the determinant of a band matrix[12] h_{ij}

$$h_{ij} = \sum_{l=0}^{M} (\partial c_i/\partial \mathbf{R}_l)\cdot(\partial c_j/\partial \mathbf{R}_l) \tag{3.13}$$

and c_i is one of the set of constrained bond lengths or angles (or opposite sides). Multiplicative constants independent of i and j in (3.13) are not important and have been omitted. In practice h can be computed rapidly, because it is a band matrix. The derivatives of h are more difficult to calculate but are required in a dynamical simulation. Therefore ln h was assumed to be (approximately) additive over successive dihedral angles, and for each dihedral angle φ_i a polynomial function of the three-bond distance $\mathbf{R}_{i+1}-\mathbf{R}_{i-2}$, fixed by the angle, was used for the compensating potential. As will be seen, this worked adequately and brought P^M into the same framework used for general nonbonded interactions.

IV. Random Force. Equations 3.1, 3.4, and 3.7 give

$$V = G[H^{-1}V^0 + P + \mathcal{R}] \tag{3.14}$$

where

$$G \equiv (H^{-1} + Q)^{-1} \tag{3.15}$$

(It is apparent from (3.15) that the simultaneous inclusion of hydrodynamic interaction and internal friction requires complicated matrix operations that may well be impractical unless preaveraging of the matrices is introduced.) The random force $\mathcal{R}$ is now required for completion of eq 3.14.

$\mathcal{R}$ is presumed to have the equivalent descriptions

$$\mathcal{R} \rightarrow -k_B T \nabla \ln \Psi \tag{3.16}$$

$$\mathcal{R} \rightarrow \text{stochastic} \tag{3.17}$$

Equation 3.16 is used in an ensemble description of the system, with $\Psi(x,t)$ the probability density at a point x in configurational phase space. In this description the velocity calculated from eq 3.14 and 3.16 is designated V^S, the Smoluchowski streaming velocity

$$V^S = G[H^{-1}V^0 + P - k_B T \nabla \ln \Psi] \tag{3.18}$$

and is used in the conservation equation

$$\partial\Psi/\partial t = -\nabla^T(V^S\Psi) \tag{3.19}$$

to determine the dynamical properties of the system. ∇^T is the transpose of the column matrix of gradient operators. Equation 3.17 is merely a reminder that the second description of $\mathcal{R}$ is stochastic. The actual properties of $\mathcal{R}$ are still to be established from the requirement of equivalence. This equivalence is tested by comparison of eq 3.18 with the corresponding streaming velocity implied by a diffusion equation derived from eq 3.14 and 3.17.

B. Difference Equation and Diffusion Equation. As in section 2, x^0 stands for the configuration at the beginning of a time step τ and x for the configuration at the end.

$$\Delta x \equiv x - x^0 = \int_0^\tau V \, dt \tag{3.20}$$

Equations 3.14 and 3.17 give

$$\Delta x = [\bar{G}\bar{H}^{-1}\bar{V}^0 + \bar{G}\bar{P}]\tau + K \tag{3.21}$$

where $\bar{G}\bar{P}$ is the time average of GP over the interval τ and

$$K \equiv \int_0^\tau G\mathcal{R} \, dt \tag{3.22}$$

The time average of products has been written as a product of time averages, which is correct for the midpoint rule but is otherwise an approximation. We assume that K is a Gaussian process, with variance proportional to τ, and that K's for successive time steps are uncorrelated. The latter property is sufficient to make x satisfy a diffusion equation for any of the integration rules to be adopted for the calculation of $\bar{G}\bar{P}$.

We consider first a very short time step.

I. Small τf. The diffusion equation for x has the general form

$$\partial\Psi/\partial t = -\nabla^T(V^L\Psi) \tag{3.23}$$

where

$$V^L = \tau^{-1}\langle\Delta x\rangle_L - \Psi^{-1}\nabla^T(D\Psi) \tag{3.24}$$

and

$$D \equiv (2\tau)^{-1}\langle\Delta x\Delta x^T\rangle_L \tag{3.25}$$

The brackets $\langle\ \rangle_L$ indicate an average over the Langevin displacements K that occur during the time interval $(0,\tau)$. The moments of Δx and K remain to be established by the equivalence requirement $V^L = V^S$.

If τ is much smaller than the vibrational relaxation times, $\bar{G}\bar{P}$ can be approximated by $G(x^0)P(x^0)$. Then a calculation of V^L from (3.21) and (3.24) gives

$$V^L = G[H^{-1}V^0 + P] + \tau^{-1}\langle K\rangle_L - \Psi^{-1}\nabla^T(D\Psi) \tag{3.26}$$

and

$$D = (2\tau)^{-1}\langle KK^T\rangle_L \tag{3.27}$$

Agreement between V^L and V^S follows from the following specification of the moments of K:

$$\langle KK^T\rangle_L = 2\tau k_B T G \tag{3.28}$$

or

$$D = k_B T G \tag{3.29}$$

and

$$\langle K\rangle_L = \tau\nabla^T D \tag{3.30}$$

In recent work we have used a divergenceless diffusion matrix, for which $\langle K\rangle_L$ vanishes. We know of no general reason why $\nabla^T D$ must vanish. Incompressibility of the solvent does not suffice except when the beads are far apart, or a relatively crude approximation to HI is being used, and internal friction is omitted.

The practical calculation of Langevin forces that satisfy eq 3.28 is considered in the accompanying paper.[23]

II. Large τf. We return now to eq 3.21 for Δx and suppose that τ remains sufficiently short that conformational displacements are very small during a time step. However, τf is now sufficiently large that vibrational degrees of freedom should have relaxed completely during the time step, and the metric potential compensation is required. A considerable apparatus has to be constructed to give formal justification to that compensation and to the remaining parts of the argument. A transformation of coordinates analogous to that used with constrained degrees of freedom[1] is necessary to distinguish vibrational coordinates (bond lengths and angles) from conformational coordinates. G, if dependent on configuration at all, would have to be taken a function only of the conformational coordinates. The construction of $P = P^V + P^E$ would likewise require that P^E be approximated by $P^E(x^0)$, since

only vibrational coordinates could change significantly during τ. However, we should be led by these transformations to exactly the formalism[1] previously constructed for constrained coordinates, with one distinction. Instead of having P^V a constraining force determined from the conditions of vanishing vibrational amplitudes, P^V would be proportional to residual vibrational displacements of very small magnitude. This distinction does not seem to warrant repetition of the previous formal arguments.

The result of the use of constraints, or of taking $\tau f >> 1$, and simultaneous retention of eq 3.28 and 3.30 for the moments of K, is that a diffusion equation is recovered for the conformational subspace of x. This equation differs, however, from the diffusion equation in the subspace that is given by eq 3.18 and 3.19. The difference is corrected by inclusion of the metric potential in P. (It is perhaps preferable to regard the correction as belonging to $\langle K \rangle_L$, since the moments of K are inferred by the requirement of equivalence.)

III. Intermediate τf. As τf moves away from the two limits, 0 and ∞, formal arguments that justify the integration rule for $\bar{G}\bar{P}$ rapidly lose force. An explicit first iteration of the trapezoidal rule may be justified by Helfand's analysis[15] as was noted in section 2. In practice it has to be left to computer "experiments" whether a given value of τ is sufficiently small to permit the use of an explicit rule, whether variation of G during a time step can be suppressed, whether f is sufficiently large to justify the metric potential compensation, and whether the implicit methods converge. The modifications are easily switched on and off in the algorithm and their consequences tested fairly readily despite the weakness of general arguments. We shall therefore go on with little additional formal justification to record the algorithm, and rely on the results of section 4 to test the merit of at least some of the options.

C. The Iterative Algorithm. The practical solution of the difference equation (3.21) will now be summarized. With suppression of internal friction, the equation has the form

$$\Delta x = x - x^0 = A + \tau \bar{H}\bar{P} \tag{3.31}$$

where

$$A \equiv \tau \bar{V}^0 + K \tag{3.32}$$

and

$$\bar{P} = \bar{P}(x^0,x) \tag{3.33}$$

The actual functional form of P for the different special cases will be summarized below. A is evaluated at the beginning of the time interval and the notation below may suggest that A is treated as a constant vector within the time interval. However, if H is updated within a time step, A must be updated as well, since the Langevin forces in A have covariance H. In practice we included the updating, when HI was used during the simulations described in section 4. But as the diagonal elements of H are constants and the off-diagonal elements are very smooth functions of x, the effect of such updating should be relatively small. It was marginal whether the changes due to updating H exceeded the statistical error of our runs.

I. Summary of Integration Rules. (a) Small τf. For small τf, the MP time integration rule (2.5) is used for all parts of the potential force P. The metric potential need not be included.

(b) Intermediate and Large τf. Here the division (3.10) of P into the vibrational part P^V and the remainder P^E is used. P^E includes the compensating metric potential, which was approximated as a sum of potentials for each dihedral angle in the dynamic part of the program.

For many problems of interest, trajectories need to be followed for an equilibrium sampling of initial positions, and a compensating metric potential is needed either in the dynamical calculation of the trajectory (to achieve conventional statistics) or in the equilibrium sampling (to achieve constrained statistics) but not in both. If the equilibrium sampling is to be biased toward constrained statistics by means of a compensating metric potential, then advantage can be taken of the narrow band structure of (3.13) to facilitate an exact and rapid calculation. However, the main results reported in section 4 incorporated the correction in the trajectory part of the calculation rather than in the equilibrium part.

The MP rule (2.5) was used for $\bar{P}^E$, and the BE rule (2.6) was used for $\bar{P}^V$. In practice, an essential feature of the successful treatment of $\bar{P}^V$ for large τf is that the iterative process allows $P^V(x^0)$ to be discarded. The BE rule satisfies this requirement, but the MP and TR rules do not. For large τf, no correlation between the values of P^V at the beginning and end of the time interval is to be expected, and initiation with $\bar{P}^V = 0$ worked as well as initiation with $\bar{P}^V = P^V(x^0)$.

II. Iterative Mechanics. The Newton–Raphson method[9] was used to solve the implicit equation (3.31) for the configurational displacement. Let x_n be the nth estimate of the final configuration x, and

$$x_{n+1} \equiv x_n - y_n \equiv x^0 - C_{n+1} \tag{3.34}$$

Thus y_n is the (negative) change in successive estimates of x_n, and C_{n+1} is the cumulative (negative) displacement. Let

$$\bar{P}_n \equiv \bar{P}(x^0,x_n) \tag{3.35}$$

The Taylor expansion

$$\bar{P}_{n+1} = \bar{P}_n - \tfrac{1}{2}J_n y_n + \ldots \tag{3.36}$$

where

$$J_n \equiv 2((\partial/\partial x_n)\bar{P}_n)^T \tag{3.37}$$

is the Jacobian (defined arbitrarily as twice the usual definition), is terminated with the displayed terms for large τf. For small τf, the Jacobian is suppressed and straightforward iteration is used as in Helfand.[15] We concentrate here on the procedure for large τf. The Jacobian derivatives of $\bar{P}_n{}^V$ form a matrix $J_n{}^V$ with a narrow band structure, which greatly facilitates the solution of the coupled linear equations for the displacements y_n. However, the derivatives $J_n{}^E$ of $\bar{P}_n{}^E$ form a full matrix, and since the elements of $J_n{}^E$ were expected to be much smaller than those of $J_n{}^V$, only the diagonal dyadic elements of $J_n{}^E$ were retained. In practice, the diagonal blocks of $J_n{}^E$ usually made a moderate improvement in the rate of convergence and were retained for greater accuracy in the test runs of section 4.

Evaluation of eq 3.31 with $x = x_{n+1}$ gives

$$(\tfrac{1}{2}\tau\bar{H}J_n - 1)y_n = a_n \tag{3.38}$$

where

$$a_n \equiv \tau\bar{H}\bar{P}_n + C_n + A \tag{3.39}$$

In the absence of HI, $\bar{H}$ is just the diagonal matrix β^{-1}, $\bar{H}J_n$ remains a narrow band matrix, and eq 3.38 is readily soluble. If HI is present, $\bar{H} = \beta^{-1} + \bar{T}$ is substituted into (3.38) and a subset of iterations is performed on

$$(\tfrac{1}{2}\tau\beta^{-1}J_n - 1)y_n{}^{m+1} = a_n - \tfrac{1}{2}\tau\bar{T}J_n y_n{}^m \tag{3.40}$$

$$(\tfrac{1}{2}\tau\beta^{-1}J_n - 1)y_n{}^0 = \tau\beta^{-1}\bar{P}_n + C_n + A \tag{3.41}$$

The alternative initiation, for which $\bar{H}$ replaces β^{-1} in the

right side of (3.41), did not converge nearly so well when HI was large. The subiterations were terminated at y_n^1 to y_n^3, depending on the magnitude of the change in y_n^m. This process was not as expensive as might be thought, because the matrix multiplying y_n^{m+1} on the left side of eq 3.40 is a band matrix that had already been factored into upper and lower triangular matrices during the calculation of y_n^0. The subiterations converged fairly well for Stokes diameters up to 1. (For still larger HI it might be advantageous to slow down the subiterative changes in y_n^{m+1} by slight admixture of y_n^m.) More than two main iterations, i.e., $n > 2$, were rarely necessary for realistic backbone potentials. However, highly softened vibrational force constants allow greater atomic displacements within the time interval and more frequently necessitated greater values of n up to 3 or 4.

Convergence was generally estimated from the magnitude of the successive changes in y_n. Computation of the actual error in the approximate solution of eq 3.31 requires almost as much information as is required for another iteration, and the actual error was well predicted by the preceding value of y_n.

III. Rescue Procedures. Although the iterative procedure just described almost always converges rapidly, it is not guaranteed to converge at all and occasionally does not if τ is very large. We believe that failure to converge occurred for those special configurations where simultaneously the nonbonded forces were very strong and the vibrational forces were very weak. In any event, convergence was always restored by the following two devices: (a) introduction of the diagonal dyadic part of J_n^E if it had been suppressed in the first attempt, and (b) halving τ. The second device requires some care in principle since the Langevin forces have to be recomputed for the subdivided interval. Simply throwing away the previously used Langevin forces would introduce an improper correlation between the Langevin forces and the configuration. In order to avoid this correlation the independent random numbers used to construct the Langevin forces were always generated for the subdivided interval. Initially they were combined and used for the full interval but were available in the event of convergence difficulties. The extra computational effort required by this provision was negligible, so no attempt was made to devise more elegant procedures. (The easiest such procedure would probably involve normally distributed random numbers, rather than the uniformly distributed ones actually used. Advantage could then be taken of the fact that the sum of two normally distributed variables also has a normal distribution.)

4. Illustrative Results

With one exception, all the tests to be discussed concern a uniform chain with 11 beads and tetrahedral bond angles. All beads separated by three or more bonds interact with an identical Lennard-Jones potential. The exception was a preliminary check of the metric potential compensation (3.12) for a four-bead chain without nonbonded interactions.

The Lennard-Jones interaction $u_{LJ}(R)$ had the standard form

$$u_{LJ}(R) = \epsilon[-(\sigma/R)^6 + (\sigma/R)^{12}] \tag{4.1}$$

(A small constant, 0.001, was added to R to avoid any possibility of numerical problems). All parameters are expressed in the units

$$\begin{aligned} &\text{length:} && b_0 \\ &\text{energy:} && k_B T \\ &\text{time:} && \beta_0 b_0^2/k_B T \end{aligned} \tag{4.2}$$

where b_0 and β_0 are reference values for bond lengths and bead friction constants, respectively. All bond lengths were chosen to have the value unity, and all friction constants were the same and were characterized by the dimensionless ratio of the Stokes diameter to b_0. The Lennard-Jones parameters were assigned values $\epsilon = 2$ and $\sigma = 1.75$. These give a significant but not insurmountable potential barrier at the cis conformation. Vibrational potentials between adjacent and next adjacent atoms along the backbone had the form

$$u(R) = \tfrac{1}{2}f(R - R_0)^2 \tag{4.3}$$

The value of R_0 was set to unity for adjacent atoms and was set to the tetrahedral bond distance $(^8/_3)^{1/2}$ for next adjacent atoms. The force constants f_b for adjacent atoms and f_θ for next adjacent atoms were adjusted to yield three sets of values for bond length and bond angle vibrations. The smallest force constants and largest fluctuations, set a, were close to those used by Helfand et al.[7] and gave root mean square bond length fluctuations of 0.056 and relative tetrahedral angle fluctuations of 0.073 for $f_b = 328.5$ and $f_\theta = 750$. These fluctuations refer to the innermost bonds, but the variation along the chain did not exceed 5% for set a and was much less for the harder vibrational potentials. Set b gave corresponding length and angle fluctuations of 0.021 and 0.036 for $f_b = 2365$ and $f_\theta = 1100$. These we regard as reasonably realistic values. Set c gave length and angle fluctuations of 0.01 and 0.014 for $f_b = f_\theta = 10^4$.

The force constants and vibrational fluctuations just described refer to equilibrium or Monte Carlo simulations or to dynamical runs with small τf. The force constants used in the Langevin steps for large τf could be chosen differently from the values used in Monte Carlo randomization, but in fact the former were always chosen to be half the latter. This choice was a fortuitous program default, rather than the result of any attempt at optimization. As it happened, the choice gave a good match between dynamical and equilibrium vibrational amplitudes where it most mattered, for the softened force constant set a, and the worst match where it mattered least, for the hardened set c.

A. Monte Carlo Three-Bond Distribution. The distribution of the dihedral angle was studied indirectly, in terms of the distribution of the distance between the ends of the four-bead chain that includes the dihedral angle. The distance distribution provides an indirect test of the dihedral angle distribution and also shows the effects of vibrational fluctuations on the cusps that appear in the distance distribution for a chain with constrained bond lengths and angles. Figure 1 shows the equilibrium distribution of distances for the innermost dihedral angle of an 11-bead chain, as determined by Monte Carlo sampling of vibrational sets a, b, and c. Figure 2 compares the distribution for set b with that for a constrained four-bead chain without nonbonded interactions. The latter distribution has singularities at the cis and trans conformations. A conspicuous remnant of the trans singularity can be seen in Figure 1 for vibrational sets b and c. However, the variation of the weights near the cis barrier is probably more significant for most purposes. The weaker the vibrational force constants, the more able is the chain to avoid the region of high repulsive potential through the intervention of bond angle fluctuations.

We note parenthetically that the acquisition of good Monte Carlo data is not a trivial problem. A combination of reptation transfers of three-bead groups from tail to head was used in conjunction with many small displacements of all beads in sequence. The small displacements are very slow to sample the conformation space, while

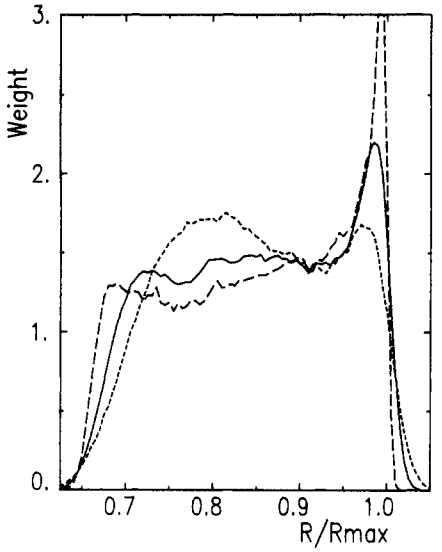

Figure 1. Monte Carlo simulation of distribution of three-bond distance enclosing the innermost dihedral angle of an 11-bead chain. R_{max} is the maximum extension in the absence of vibrational fluctuations. Short-dashed curve gives results for the softened vibrational force constant set a, solid curve is for the realistic set b, and medium-dashed curve is for the hardened set c.

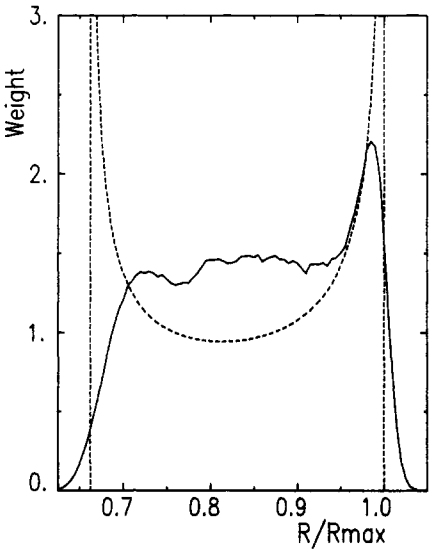

Figure 2. Solid curve is Monte Carlo simulation of vibrational set b, as in Figure 1, and dashed curve is analytical distribution for constrained chain in the absence of nonbonded interactions.

reptation attempts involving only a single bead are virtually nonergodic with respect to equilibration of the different weights for interior and end dihedral angles. (The trans conformation is relatively more favorable for end beads compared to interior ones, as a result of the nonbonded interactions.)

B. Dynamical Three-Bond Distribution. We consider next the ability of the dynamical algorithm to reproduce the equilibrium distributions shown in Figure 1 and the corresponding distributions for the end dihedral angle. Results will be shown only for the implicit algorithm used for large τf. However, extensive comparisons were made with results for short time steps, for which the implicit method becomes explicit and reduces in all essentials to that of Helfand.[7,15] The comparison provided measures of relative accuracy and computational cost. Also, results are displayed primarily for chains with strong HI, as providing a more complete test of the methods.

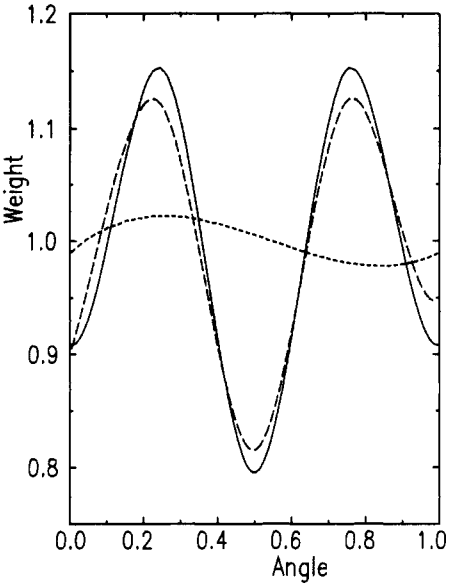

Figure 3. Relative weights vs. dihedral angle for three-bond chain without nonbonded interactions. The trans conformation is reached at angle values 0 and 1 and the cis conformation at 0.5. The solid curve is the analytical result, the medium-dashed curve is dynamical simulation for $\tau = 0.01$ without metric potential compensation, and the short-dashed curve is with compensation. The simulation curves are spline fits with standard deviations of 0.02–0.03 from the raw data.

A preliminary test of the metric potential compensation was performed on a four-bead chain with large vibrational force constants, set c, and without nonbonded interactions or HI. Figure 3 shows the distribution of dihedral angle that is obtained analytically for a rigidly constrained chain[12] in comparison with the distribution obtained from the dynamical algorithm for 200 steps with $\tau = 0.01$, with and without the compensating metric potential. The distribution for an unconstrained chain should be uniform and should equal the displayed analytical curve for a constrained chain. The implicit algorithm gives reasonably good agreement with the constrained distribution if the metric potential is not included and with the uniform distribution when the compensating potential is included.

We return now to the three-bond distance distribution for the innermost and terminal dihedral angles of an 11-bead chain for vibrational sets a, b, and c. The distributions for dynamical runs are shown in Figures 4–9, in comparison with the distributions obtained by Monte Carlo sampling. The dynamical runs all used trajectories of 200 steps with step length $\tau = 0.01$ and included HI with a Stokes diameter of unity. The dynamical curves are averages over 200–400 trajectories. Each trajectory was sampled at the end of each time step and the initial configuration of a trajectory was chosen by the Monte Carlo method.[24]

The comparison between Monte Carlo and dynamical runs is generally encouraging. The shift in the distribution functions between terminal and interior dihedral angles, and between vibrational force constant sets a, b, and c, is followed rather well. The mean square end-to-end distance $\langle L^2 \rangle$ was also tabulated; the Monte Carlo values were 17.0, 17.4, and 18.3 for vibrational sets a, b, and c, respectively, and 15.9, 17.5, and 17.5 for the dynamical runs. Similar discrepancies in $\langle L^2 \rangle$ were found for runs with small τ on sets a ($\tau = 4 \times 10^{-4}$) and b ($\tau = 2 \times 10^{-4}$). (We note that the weakening of force constants is not completely effective in allowing larger τ; the increased motion permitted by the larger vibrations required smaller values of τf for similar error requirements.)

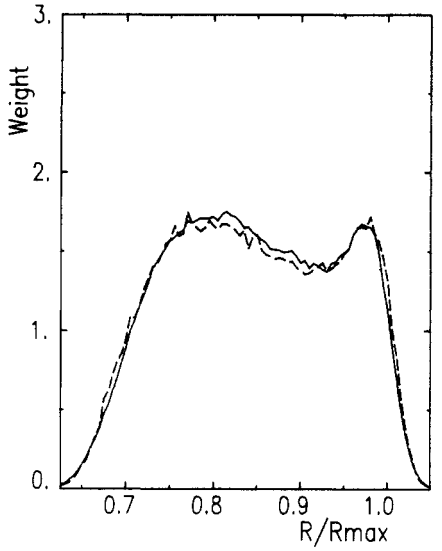

Figure 4. Relative weights vs. R/R_{max} as in Figure 1. Innermost dihedral angle, vibrational set a. The solid curve is from Monte Carlo simulation and the dashed curve is from the dynamical implicit algorithm with $\tau = 0.01$.

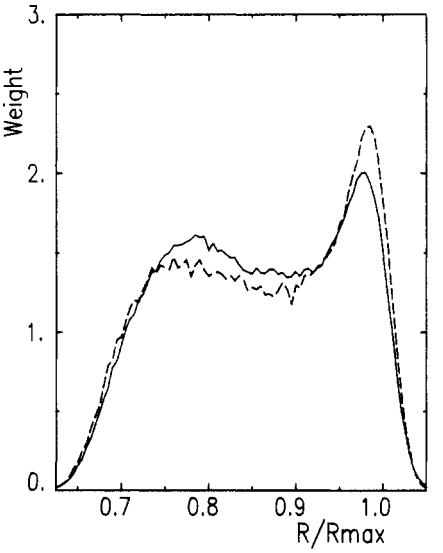

Figure 5. Same as Figure 4 for terminal dihedral angle of vibrational set a.

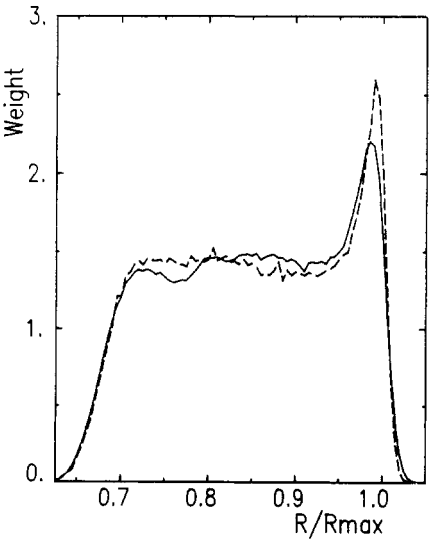

Figure 6. Same as Figure 4 for innermost dihedral angle of vibrational set b.

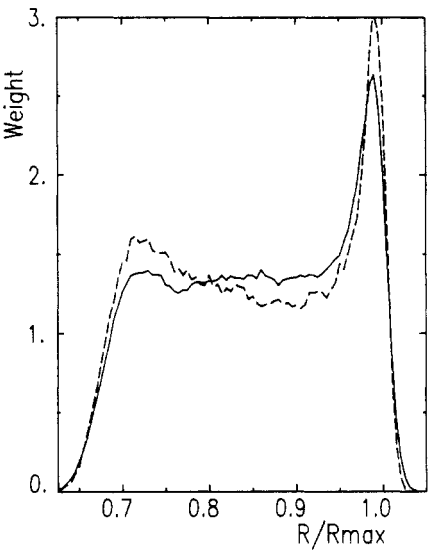

Figure 7. Same as Figure 4 for terminal dihedral angle of vibrational set b.

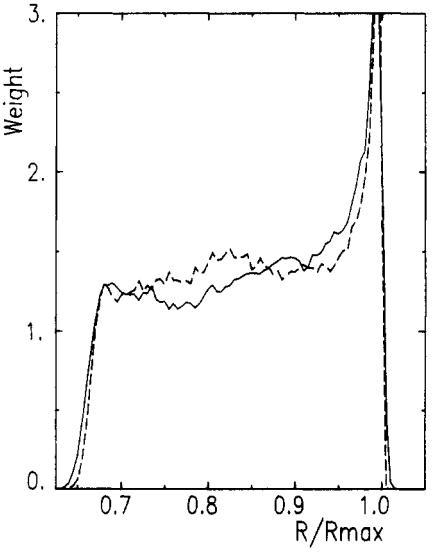

Figure 8. Same as Figure 4 for innermost dihedral angle of vibrational set c.

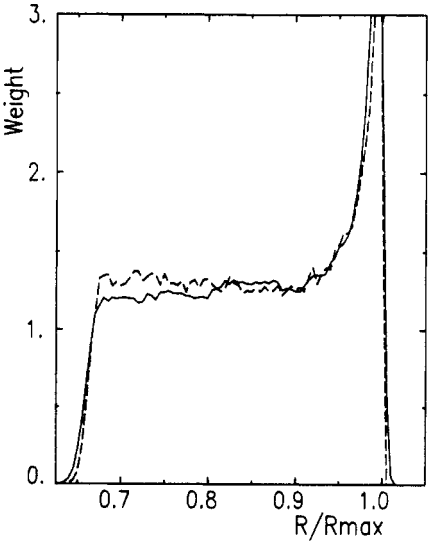

Figure 9. Same as Figure 4 for terminal dihedral angle of vibrational set c.

Some of the discrepancies between Monte Carlo and dynamical results in Figures 4–9 seemed to be reasonably

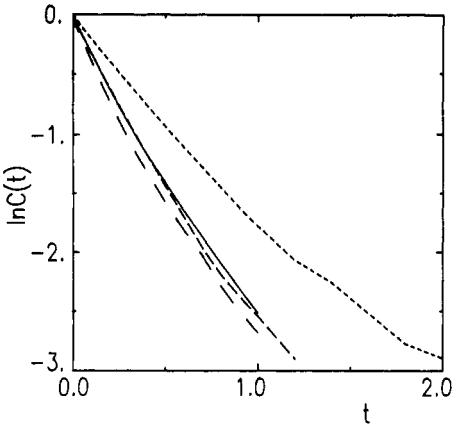

Figure 10. Dynamical simulations of end bisector time correlation function. The solid curve is for vibrational set b with $\tau = 2 \times 10^{-4}$, the medium-dashed curve is for vibrational set b with $\tau = 0.01$, the short-dashed curve is the same as the medium-dashed curve except that HI is added. The long-dashed curve is for vibrational set a with $\tau = 4 \times 10^{-4}$.

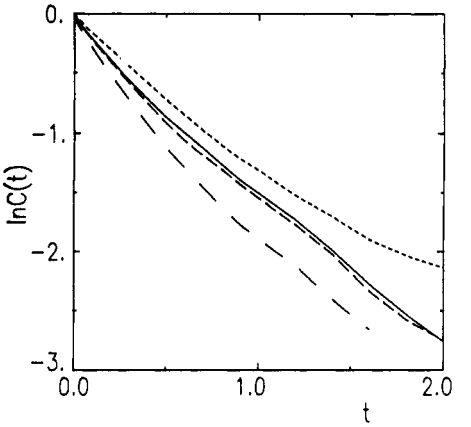

Figure 11. Same as Figure 10 except that second bisector from end was used.

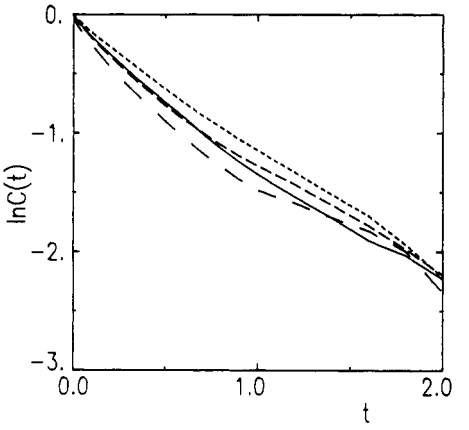

Figure 12. Same as Figure 10 except that third bisector from end was used.

predictable from the magnitudes of vibrational fluctuations, specifically the degree of broadening of the cusp at large R and the response to the barrier at small R. However, those discrepancies seemed relatively small. Net shifts in the weights, as seen in Figure 5, for example, were not predictable but were generally greater for terminal dihedral angles than interior ones and slightly less, for the terminal angles, for runs without HI on the same random number set. The last effect may be due simply to the fact that large HI slows down the equilibration of end beads considerably but has relatively small effect on motion of the interior dihedral angle. The overall discrepancies between runs with and without HI were noticeably smaller than those shown in Figures 4–9, so we believe that moderately large HI can be handled adequately by the explicit algorithm.

For the 11-bead chains the explicit algorithm covered a trajectory of total duration $t = 2$ about 6–7 times faster than the explicit or short-τ algorithm for vibrational set a (6 for strong HI, 7 for no HI), and about 12 times faster for set b. A few trial runs on 50-bead chains indicated a near doubling of the speed ratios. For either the explicit or implicit algorithms, inclusion of HI approximately doubled the computation time.

C. Dynamical Time Correlations. We consider next the time correlation

$$C(t) = \langle \mathbf{l}(t) \cdot \mathbf{l}(0) \rangle / \langle |\mathbf{l}(0)|^2 \rangle \qquad (4.4)$$

where $\mathbf{l}(t)$ is the bisector of an adjacent pair of bonds. The integral of $C(t)$ would correspond closely to a relaxation time obtained from magnetic resonance. Figures 10–12 give results for the first three bisectors starting from the chain end. Results for the dynamical simulation with small time steps are shown for vibrational sets a and b, without HI, and for large time steps with and without HI for set b. The run with HI again used a Stokes diameter of unity.

The differences between vibrational sets a and b seem rather small and are in rough agreement with expectations, considering that results for large t have considerable statistical uncertainty. The softened vibrational set a shows slightly faster relaxation, at least for short times, than does set b, and HI slows up the relaxation slightly for set b. The runs on set b using the explicit and implicit algorithms (the solid and medium-dashed curves, respectively) should give the same results. The agreement lies within the statistical uncertainty, and the implicit algorithm ran through the trajectory about 12 times faster.

5. Application to Interacting Chains

In most respects the application of the implicit algorithm to interacting chains presents no difficulty. Considerable work has been carried out for rodlike polymers.[25,26] The distinction between one chain and many chains need consist only in the specification of vanishing vibrational force constants in the input data periodically along the chain and an appropriate choice of initial configuration. The use of periodic boundary conditions requires a shift of relative centers of force to the closest image separation prior to the computation of the force. For the simulation of rodlike polymers, or of any bonds much greater in length than the range of the force, it is advantageous to replace the interaction between point centers of force by an interaction between bonds. This amounts to the use of pair interactions, each of which depends on the coordinates of four endpoints, namely the two ends of each of the interacting bonds.

More serious problems are presented by the accommodation of periodic boundary conditions to hydrodynamic interaction. The latter is very long ranged, and no partial summation of the interaction over images is likely to be satisfactory. An analytical and physically motivated treatment of distant contributions is required. This has not yet been attempted.

References and Notes

(1) Fixman, M. *J. Chem. Phys.* **1978**, *69*, 1527.
(2) Fixman, M. *J. Chem. Phys.* **1978**, *69*, 1538.
(3) Pear, M. R.; Weiner, J. H. *J. Chem. Phys.* **1979**, *71*, 212.
(4) Ryckaert, J.-P.; Ciccotti, G.; Berendsen, H. J. C. *J. Comput. Phys.* **1977**, *23*, 327.
(5) van Gunsteren, W. F.; Berendsen, H. J. C. *Mol. Phys.* **1977**, *34*, 1311.

(6) Ciccotti, G.; Ferrario, M.; Ryckaert, J.-P. *Mol. Phys.* **1982**, *47*, 1253.
(7) Helfand, E.; Wasserman, Z. R.; Weber, T. A. *Macromolecules* **1980**, *13*, 526.
(8) Hall, G., Watt, J. M., Eds. "Modern Numerical Methods for Ordinary Differential Equations"; Oxford University Press: Oxford, 1976.
(9) Dahlquist, D.; Bjorck, A. "Numerical Methods"; Prentice-Hall: Englewood Cliffs, NJ, 1974.
(10) In connection with the applicability of methods devised for systems of stiff differential equations, we acknowledge a stimulating workshop on the subject of time scales in simulations, organized by H. J. C. Berendsen in Oct 1982.
(11) The only difference is that nonbonded interactions are handled more accurately by the midpoint rule used in the implicit algorithm.
(12) Fixman, M. *Proc. Natl. Acad. Sci. U.S.A.* **1974**, *71*, 3050.
(13) Helfand, E. *J. Chem. Phys.* **1979**, *71*, 5000.
(14) Ermak, D. L.; McCammon, J. A. *J. Chem. Phys.* **1978**, *69*, 1352. Fixman, M. *Macromolecules* **1981**, *14*, 1710. Fixman, M. *J. Chem. Phys.* **1983**, *78*, 1594.
(15) Helfand, E. *Bell Syst. Tech. J.* **1979**, *58*, 2289.
(16) The methods used here for strong nonbonded interactions retain only diagonal blocks in the nonbonded contribution to the Jacobian and worked rather well. A similar approach to the forces that attach side chains to the backbone might be satisfactory and would require no significant modification of the implicit algorithm.
(17) Gottlieb, M.; Bird, R. B. *J. Chem. Phys.* **1976**, *65*, 2467.
(18) Verlet, L. *Phys. Rev.* **1967**, *159*, 98.
(19) Zwanzig, R. *Adv. Chem. Phys.* **1969**, *15*, 325.
(20) Rotne, J.; Prager, S. *J. Chem. Phys.* **1969**, *50*, 4831.
(21) Fixman, M. *J. Chem. Phys.* **1982**, *76*, 6124.
(22) Cerf, R.; *C. R. Acad. Sci.* **1982**, *294*, 769.
(23) Fixman, M. *Macromolecules* **1986**, *19*, following paper in this issue.
(24) The Monte Carlo method of initialization may have led to some bias favoring agreement with Monte Carlo results. However, the total duration of a trajectory was about twice the relaxation time for the slowest dihedral angle relaxation. In practice this was ample time for the trajectories to go astray as a result of programming error or failure to require adequate convergence of iterations. Errors could be seen not only in the dihedral angle distribution but also in the mean square end-to-end distance. The distribution of a dihedral angle, or of the three-bond distance controlled by the angle, is a more sensitive test of iteration accuracy than the end-to-end vector and equilibrates more rapidly.
(25) Fixman, M. *Phys. Rev. Lett.* **1985**, *54*, 337.
(26) Fixman, M. *Phys. Rev. Lett.* **1985**, *55*, 2429.

Construction of Langevin Forces in the Simulation of Hydrodynamic Interaction†

Marshall Fixman

Department of Chemistry, Colorado State University, Fort Collins, Colorado 80523.
Received October 7, 1985

ABSTRACT: In the simulation of Brownian motion with hydrodynamic interaction, the construction of Langevin forces with the proper covariance is by far the slowest operation for large systems if standard, numerically exact methods are used. An approximate method with controlled accuracy is presented that considerably reduces the computation required for the construction of such forces.

1. Introduction

The problem being considered here is the calculation of random numbers y_i that are proportional to the Langevin forces.[1] The y_i have a covariance matrix

$$\langle y_i y_j \rangle = H_{ij} \tag{1.1}$$

where H_{ij} is an element of the (positive-definite) hydrodynamic interaction (HI) or diffusion matrix H. The H_{ij} are function of configuration. There are (at least) two ways of satisfying (1.1). Each starts with a factorization of H

$$H = A^{\mathrm{T}}A \tag{1.2}$$

The properties of A will be discussed below. A^{T} is the transpose of A. If A^{T} is available, the construction

$$y = A^{\mathrm{T}}x \tag{1.3}$$

where

$$\langle x_i x_j \rangle = \delta_{ij} \tag{1.4}$$

is readily verified to satisfy (1.1). y and x are the column matrices composed of y_i and x_i, respectively.

In libraries of mathematical and statistical algorithms, a Choleski factorization[3] of H is commonly used. In this method A is an upper triangular matrix, and of course A^{T} is lower triangular. If H is an $M \times M$ matrix, construction of A takes $M^3/3$ arithmetic operations.[3] In principle A has to be constructed anew for each time step, and the explicit calculation of A is a serious problem for large systems.

It may be that HI is worth including only for large-scale motions of the system, since the physical models and calculations will not be very realistic for local (small-scale) motion. And fortunately the effect of HI on local motion is usually a small correction to the motion induced by potential forces and unperturbed frictional forces due to the solvent. An approximation might then be used in which M is cut down to ca. $3x$ (10 centers of friction) and the standard method followed. Such approximations are not obviously valid, and considerably larger values of M may be necessary, for example, in a theoretical study of the coupling between global and local motion, and the standard method will be very slow. The approximate method to be described allows a much faster calculation and also gives a controlled and uniform accuracy for all motions of the chain. However, it is also possible to impose a nonuniform accuracy that favors large-scale motions, if this is thought to be sufficient. This approach, as opposed to a reduction in the number of forces that perturb solvent motion, requires no tampering with the basic algorithm.

The second approach is to construct S, the square root of H, and take $A = A^{\mathrm{T}} = S$. This approach is not obviously better, because there is no available construction of the square root that is faster than the Choleski factorization of H. Iterative methods have to be used for the calculation of S, and each iteration takes about M^3 steps. Nevertheless, the square root calculation has a major potential advantage for large M. The advantage is that approximation methods can be applied directly to y rather than

† Supported in part by NIH GM27945.

0024-9297/86/2219-1204$01.50/0